Triplet–triplet annihilation-based photon-upconversion to broaden the wavelength spectrum for photobiocatalysis

Hwang, Se Yeun; Song, Dayoon; Seo, Eun Ji; Hollmann, Frank; You, Youngmin; Park, Jin Byung

DOI
10.1038/s41598-022-13406-8

Publication date
2022

Document Version
Final published version

Published in
Scientific Reports

scientific reports

Check for updates

OPEN

Triplet–triplet annihilation-based photon-upconversion to broaden the wavelength spectrum for photobiocatalysis

Se-Yeun Hwang[1,4], Dayoon Song[2,4], Eun-Ji Seo[1], Frank Hollmann[3], Youngmin You[2]✉ & Jin-Byung Park[1]✉

Photobiocatalysis is a growing field of biocatalysis. Especially light-driven enzyme catalysis has contributed significantly to expanding the scope of synthetic organic chemistry. However, photoenzymes usually utilise a rather narrow wavelength range of visible (sun)light. Triplet–triplet annihilation-based upconversion (TTA-UC) of long wavelength light to shorter wavelength light may broaden the wavelength range. To demonstrate the feasibility of light upconversion we prepared TTA-UC poly(styrene) (PS) nanoparticles doped with platinum(II) octaethylporphyrin (PtOEP) photosensitizer and 9,10-diphenylanthracene (DPA) annihilator (PtOEP:DPA@PS) for application in aqueous solutions. Photoexcitation of PtOEP:DPA@PS nanoparticles with 550 nm light led to upconverted emission of DPA 418 nm. The TTA-UC emission could photoactivate flavin-dependent photodecarboxylases with a high energy transfer efficiency. This allowed the photodecarboxylase from *Chlorella variabilis* NC64A to catalyse the decarboxylation of fatty acids into long chain secondary alcohols under green light (λ = 550 nm).

Photobiocatalysis is a rapidly growing field of biocatalysis[1–5]. Phototrophic microorganisms[6,7], light-induced enzyme reactions[8–15], and light-driven cofactor regeneration systems[16,17] have contributed to expanding the toolbox of biocatalysis for organic synthesis. Light-driven transformations have opened up new avenues for the environmentally benign synthesis of chemicals[1–5,8–10,15,18–20] and fuels[21–23].

Envisioning solar power to fuel the promising approaches mentioned above, however, is limited by the generally narrow use of the photon energy provided by sunlight. For example, reactions using flavin photocatalysts efficiently utilise wavelengths between 300 and 500 nm thereby leaving a significant part of solar energy unused.

Light upconversion (UC) possibly solves this issue. UC comprises the generation of higher-energy photons from low-energy photons (Figure S1)[24–28]. Upconverted light can be generated by combining two-photon absorption dyes, nanoparticles doped with rare-earth elements and triplet–triplet annihilation-based UC (TTA-UC) materials[29]. Among the systems, TTA-UC has been used most extensively, because the light upconversion could be achieved with non-coherent and low-power photons, to a rather high quantum efficiency (Φ_{UC}) of 1–5%[30–32]. TTA-UC has been used for photocatalysis[30,33–35], solar energy harvesting[36], drug delivery and activation[37], and luminescence bioimaging[38–40].

Established TTA-UC systems however are not compatible with aqueous reaction conditions[41], which can be solved by incorporation of the TTA-UC components into the inner space within water-stable materials[27,42]. This may allow to enhance the quantum efficiency (Φ_{UC}) because both triplet–triplet energy transfer and TTA can be accelerated via close contacts among the TTA-UC components (Figure S2).

In this study, we have prepared TTA-UC poly(styrene) (PS) nanoparticles which were doped with a platinum(II) octaethylporphyrin (PtOEP) photosensitiser and the 9,10-diphenylanthracene (DPA) annihilator (PtOEP:DPA@PS) for application in aqueous reaction systems (Figure S2). Photoexcitation of PtOEP:DPA@PS nanoparticles with 550 nm light lead to an upconverted emission of DPA at 418 nm. Hence, an unproductive wavelength for e.g. flavin excitation can be upconverted to a wavelength lying in the productive wavelength range.

[1]Department of Food Science and Biotechnology, Ewha Womans University, Seoul 03760, Republic of Korea. [2]Division of Chemical Engineering and Materials Science, and Graduate Program in System Health Science and Engineering, Ewha Womans University, Seoul 03760, Republic of Korea. [3]Department of Biotechnology, Delft University of Technology, Van der Maasweg 9, 2629 HZ Delft, The Netherlands. [4]These authors contributed equally: Se-Yeun Hwang and Dayoon Song. ✉email: odds2@ewha.ac.kr; jbpark06@ewha.ac.kr

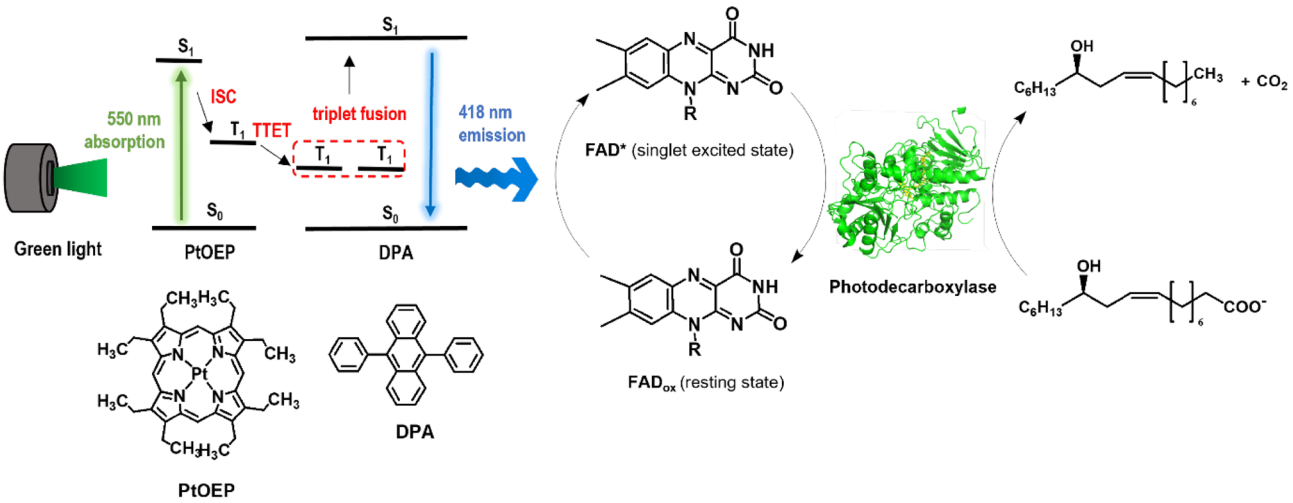

Figure 1. Overall concept of triplet–triplet annihilation-based photon-upconversion (TTA-UC) for light-driven enzyme catalysis. The TTA-UC allows conversion of long wavelength ($\lambda = 550$ nm) to short wavelength light ($\lambda = 418$ nm), which activates FAD in the enzymes for catalysis (see the Figures S1 and S2 for details). PtOEP: platinum(II) octaethylporphyrin, DPA: 9,10-diphenylanthracene, ISC: intersystem crossing, TTET: triplet–triplet energy transfer.

To test our hypothesis, we chose the light-activated fatty acid decarboxylase from *Chlorella variabilis* NC64A (*Cv*FAP)[18,43]. *Cv*FAP utilises a flavin cofactor, which in its photactivated form initiates the decarboxylation of carboxylic acids. As established previously, *Cv*FAP can productively use wavelengths between 300 and 500 nm. Green light barely promotes *Cv*FAP-catalysis. *Cv*FAP and its mutants catalyse the irreversible decarboxylation of saturated and unsaturated fatty acids but also hydroxy fatty acids[15,18], amino fatty acids, and ester bond-containing fatty acids (e.g., (*Z*)-11-(heptanoyloxy)undec-9-enoic acid)[19], generating long chain secondary alcohols, long chain aliphatic amines and esters, respectively. Engineered variants of *Cv*FAP have been reported for the conversion of short-chain carboxylic acids[22] as well as for the kinetic resolution of some α-substituted carboxylic acids and unnatural amino acid phosphinothricin[11,44].

Overall, we envision UP to enlarge the wavelength scope of photo(bio)catalytic transformations such as the *Cv*FAP-catalysed carboxylic acid decarboxylation (Fig. 1).

Results and discussion

Light upconversion by PS nanoparticles. TTA-UC nanoparticles were prepared by flash nanoprecipitation of 1.0 mL THF containing 1.0 wt% PS, 0.01 wt% PtOEP and 0.2 wt% DPA in stirred 9.0 mL milli-Q[45]. The PS nanoparticles were purified by repeated centrifugation and decantation of the supernatant. The prepared nanoparticles were spherical with an average diameter of 275 nm (Figure S3). Efficiencies for encapsulation of PtOEP and DPA in PS were determined by UV–vis absorption spectroscopy to be 29% and 24%, respectively (Figure S4 and Methods). These values correspond to molar concentrations of 3.5 μM (0.53 wt% relative to polymer) and 130 μM (8.9 wt% relative to polymer) for PtOEP and DPA, respectively. The TTA-UC nanoparticle suspension was stable for several days in air-equilibrated milli-Q water.

The PtOEP:DPA@PS nanoparticles exhibited blue emission with a peak wavelength of 418 nm, upon photoexcitation of PtOEP at a wavelength of 550 nm (Fig. 2a). The 418 nm emission was from DPA, because an identical emission spectrum was observed under direct photoexcitation of DPA at a wavelength of 394 nm. Note that 10 μM DPA (THF) did not produce fluorescence emission upon direct excitation at a wavelength of 550 nm, which rules out any unimolecular multi-photon fluorescence mechanism (Figure S5). The photoluminescence excitation spectrum of the 418 nm emission possessed substantial contributions of PtOEP, corroborating the TTA-UC mechanism (Figure S6). The corresponding anti-Stokes shift was 5807 cm^{-1}, typical of upconverted emission.

This UC emission involves two-photon processes, as seen from the quadratic dependence of its intensity on the photoexcitation power < 0.4 mW cm^{-2} (sky-blue region in Fig. 2b). The emission intensity became linearly proportional to the photoexcitation power > 0.4 mW cm^{-2} because the limiting step of TTA-UC changes from the bimolecular TTET or TTA processes to the unimolecular fluorescence transition (yellow region in Fig. 2b). The threshold photoexcitation power (i.e., 0.4 mW cm^{-2}) is one order of magnitude smaller than those of the similar polymer UC nanoparticles of PtOEP and DPA[46,47]. The lower threshold photoexcitation power can be ascribed to the increased concentrations of the PtOEP and DPA dopants, specifically resulting in enhanced triplet–triplet energy transfer. The threshold photoexcitation power and the maximum upconversion efficiency remains invariant to repetitive photoexcitation (Figure S7), which rules out photodegradation. The Φ_{UC}, which was determined using a rhodamine B standard[48], was found to increase in proportion with the photoexcitation power, and reached a saturated value of 2.1% (Figure S9 and Methods). The Φ_{UC} remained 2.0% under the photocatalysis reaction condition described below (i.e., a distance of 10 cm from the photon source (Xe lamp) and a photoexcitation power of 2.8 mW cm^{-2}). The threshold photoexcitation power and Φ_{UC} remained the same

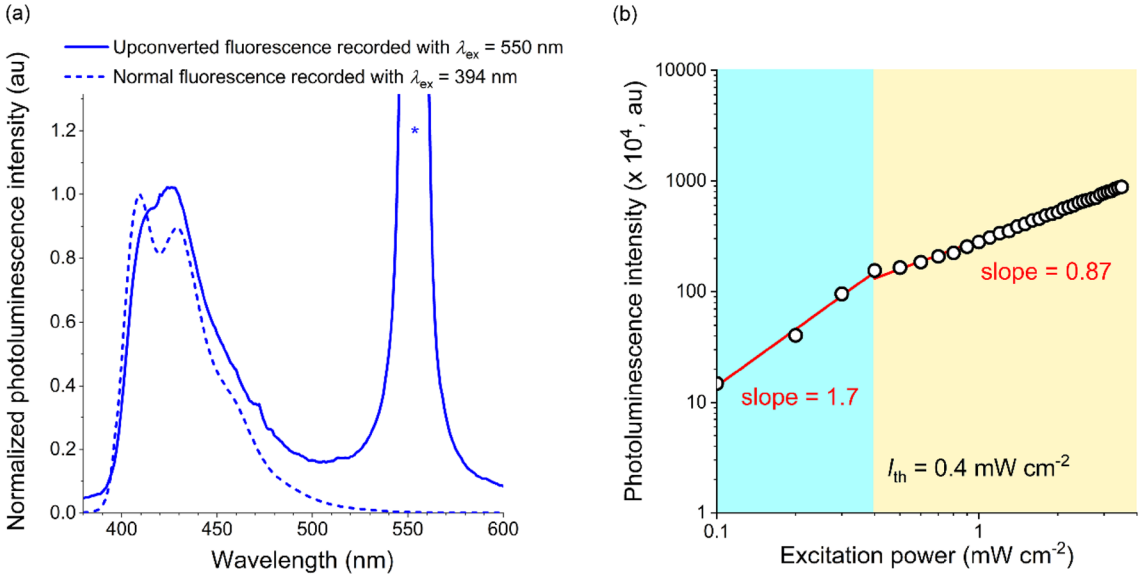

Figure 2. Upconverted fluorescence emission from TTA-UC nanoparticles. (**a**) Photoluminescence spectra of the TTA-UC nanoparticle (i.e., PtOEP:DPA@PS nanoparticle) suspension (milli-Q water) recorded upon the photoexcitation of PtOEP at a wavelength of 550 nm (solid line) and the direct photoexcitation of DPA at a wavelength of 394 nm (dashed line). The peak marked with an asterisk is the 550 nm excitation beam. (**b**) A double-logarithmic plot of the photoluminescence intensity as a function of the excitation power. The sky-blue and the yellow regions indicate upconverted fluorescence where the bimolecular TTA and the unimolecular radiative decay of DPA dominate.

regardless of the presence of O_2, indicating the high versatility of our system to the photoenzymatic reactions under aerobic conditions (Figure S8). The corresponding UC fluorescence brightness (η_{UC}) was calculated to be 29 M^{-1} cm^{-1} with the relationship, $\eta_{UC} = \varepsilon_{ex} \times \Phi_{UC}$, where ε_{ex} is the molar absorbance at 550 nm (1470 M^{-1} cm^{-1}).

Energy transfer from PS nanoparticles to *Cv*FAP. To evaluate the photoactivation ability of PtOEP:DPA@PS, we performed fluorescence titration experiments. There was a substantial spectral overlap between the DPA emission and the FAD absorption spectra (Figure S5), which suggests an occurrence of resonance energy transfer from PtOEP:DPA@PS to the FAD-binding enzyme, *Cv*FAP. Indeed, the TTA-UC fluorescence intensity of PtOEP:DPA@PS decreases with the increased concentration of *Cv*FAP (0–42 μM) (Fig. 3a). Figure 3b depicts the corresponding *Cv*FAP fluorescence titration isotherm plotting $I_0/(I_0 - I)$, where I_0 and I are the integrated intensities of TTA-UC fluorescence in the absence and presence, respectively, of *Cv*FAP, as a function of an inverse of the added enzyme concentration (i.e., 1/[*Cv*FAP]). An apparent linear dependence between the two parameters was observed, which was analysed following the Lehrer's modification of the Stern–Volmer equation (Lehrer equation, hereafter): $I_0/(I_0 - I) = 1/f + 1/(f \times k_Q \times \tau \times [CvFAP])$. In this equation, f is the attenuation factor that accounts for the accessible fraction of the energy donor (i.e., DPA), k_Q is the bimolecular rate constant for quenching of TTA-UC fluorescence via energy transfer, and τ is the lifetime of the TTA-UC fluorescence determined through time-correlated single-photon-counting techniques (42 μs; Figure S10). Linear fitting of the titration isotherm to the Lehrer equations returned f and k_Q values of 0.69 and 3.1×10^9 M^{-1} s^{-1}, respectively.

TTA-UC fluorescence titration experiments were also conducted with free FAD, instead of *Cv*FAP (Figure S11). Free FAD produced the f value (0.83) greater than f (0.69) of *Cv*FAP, which indicated strong adhesion of *Cv*FAP at the surface of PtOEP:DPA@PS nanoparticles. This adhesion is beneficial for acceleration of energy transfer, as evidenced by the k_Q value (3.1×10^9 M^{-1} s^{-1}) of *Cv*FAP greater than that (0.81×10^9 M^{-1} s^{-1}) of FAD. The efficiency of energy transfer (Φ_{ET}) from TTA-UC nanoparticles to *Cv*FAP was estimated with the relationship, $\Phi_{ET} = (k_Q \times \tau \times [CvFAP])/(1 + k_Q \times \tau \times [CvFAP])$ to be 57%. This Φ_{ET} value is two-fold greater than that with free FAD (25%).

We also investigated energy transfer behaviors of free DPA (37 μM in THF) and DPA doped in PS nanoparticles (37 μM in PS) with FAD (Figure S2). Our analyses with the standard Stern–Volmer equation revealed that doped DPA exhibited an Φ_{ET} value (29%) greater than that (13%) of free DPA (Figure S12). This improvement was likely ascribed to delocalisation of DPA exciton within the PS nanoparticles, and demonstrated the benefit of the nanoparticle approach. Collectively, our spectroscopic investigations revealed a high photoactivation ability of the TTA-UC nanoparticles.

Enzyme reactions under green light. The decarboxylation of ricinoleic acid (**1**) into (*Z*)-heptadec-9-en-7-ol (**2**) was used as a model reaction to examine application of TTA-UC for photoactivation of flavin-dependent photodecarboxylase (i.e., *Cv*FAP) (Fig. 1). After *Cv*FAP was added into the reaction medium containing 10 μM DPA in the form of ternary PtOEP:DPA@PS nanoparticles and 5 mM reaction substrates (**1**), green light

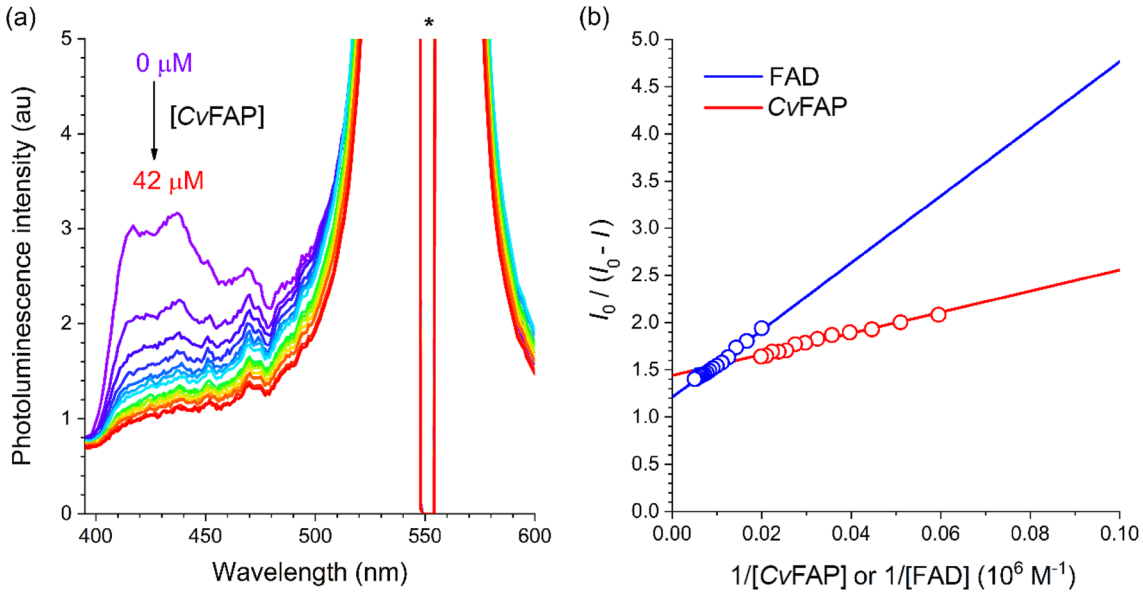

Figure 3. Photoactivation of a flavin-dependent photodecarboxylase. (**a**) Fluorescence titration results for the PtOEP:DPA@PS nanoparticle suspension (milli-Q water) recorded with increasing the concentration of a flavin-dependent photodecarboxylase (i.e., *Cv*FAP) (0–42 μM). The huge peak marked with an asterisk is the excitation beam (550 nm). See SI, Figure S11 for the titration results for free FAD. (**b**) Lehrer plot which depicts the corrected fluorescence intensity of the upconverted emission of the PtOEP:DPA@PS nanoparticle suspension (i.e., $I_0/(I_0-I)$, where I_0 and I are the integrated values of the upconverted fluorescence intensities in the absence and presence, respectively, of *Cv*FAP or FAD) as functions of 1/[*Cv*FAP] and 1/[FAD], where [*Cv*FAP] and [FAD] are molar concentrations of *Cv*FAP and FAD, respectively.

Enzyme types	[Product (2)] (μM)		TON of DPA	TON of *Cv*FAP
	w/o PtOEP:DPA@PS	With PtOEP:DPA@PS		
Purified[a]	140 ± 28	290 ± 50	15	25
Whole-cells[b]	550 ± 45	980 ± 40	86	72
	550 ± 45	1300 ± 104	50	125

Table 1. Conversion of ricinoleic acid (**1**) into (*Z*)-heptadec-9-en-7-ol (**2**) by *Cv*FAP under green light. [a]The reactions were performed by the purified *Cv*FAP in the absence and presence of the PtOEP:DPA@PS nanoparticles, which are involved in light upconversion from green to blue light. Reaction conditions: *c*(Ricinoleic acid) = 5 mM, *c*(*Cv*FAP) = 6 μM, *c*(DPA) = 10 μM, illumination with green light (λ = 550 nm). [b]The reactions were performed by the recombinant *E. coli* cells expressing *Cv*FAP in the absence and presence of the PS nanoparticles. Reaction conditions: *c*(Ricinoleic acid) = 5 mM, *c*(*E. coli*) = 7.2 g_{CDW} L^{-1} (*c*(*Cv*FAP) = ca. 6 μM), *c*(DPA) = 5 μM (up) or 15 μM (down). The TONs were calculated based on the product concentration at t = 420 min.

(λ = 550 nm) was applied by a Xe lamp (Figure S13). The decarboxylation products (**2**) were detected to 0.29 mM in the reaction medium at t = 420 min by GC/MS analysis (Table 1 and Figure S14a). This result indicated that the green light was upconverted into blue light (λ = 418 nm) by the PtOEP:DPA@PS nanoparticles, which led to photoexcitation of the FAD of *Cv*FAP and subsequently decarboxylation of ricinoleic acid (**1**) into (*Z*)-heptadec-9-en-7-ol (**2**).

The fatty alcohol (i.e., (*Z*)-heptadec-9-en-7-ol (**2**)) was also observed to 0.14 mM in the reaction medium without the nanoparticles (Figure S14b), suggesting that FAD of *Cv*FAP might be activated by green light irradiated by the Xe lamp. The turnover number (TON) of DPA in the nanoparticles and the enzyme was calculated to 15 and 25, respectively (Table 1), meaning that the light upconversion was 15 times achieved per molecule of DPA.

The TON of *Cv*FAP (Table 1) was low in the light upconversion system as compared to the blue light-based reaction system[18]. One of the reasons may include formation of the reactive oxygen species (ROS) during light upconversion[41], which may cause deactivation of the enzymes via oxidation of the sulfur-containing amino acids (e.g., cysteine 432, which is involved in catalysis)[49].

Whole-cell reactions under green light. Aiming at improving the enzyme reaction rates and TONs under green light, recombinant *E. coli* cells, which provide the ROS quenching systems (e.g., glutathione per-

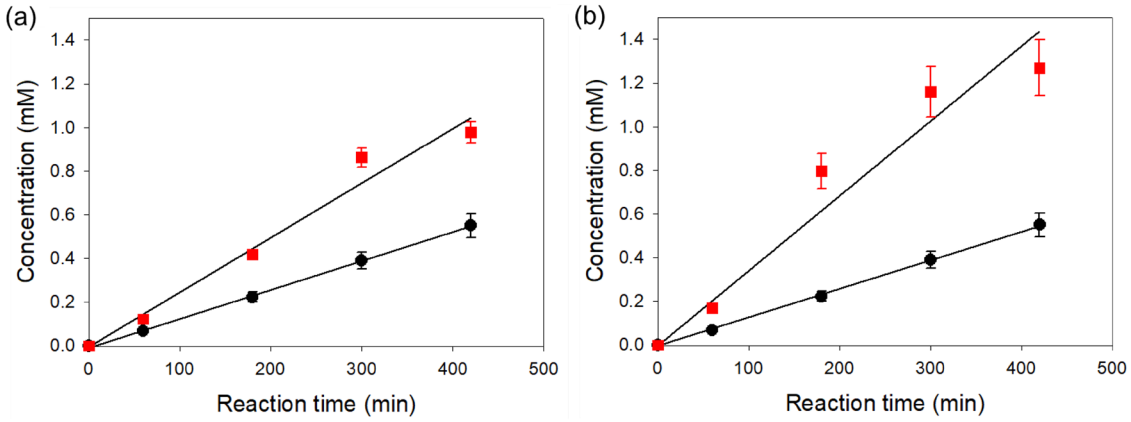

Figure 4. Time course of photodecarboxylations. Decarboxylation of ricinoleic acid (**1**) into (*Z*)-heptadec-9-en-7-ol (**2**) was carried out by the recombinant *E. coli* cells expressing *Cv*FAP under green light ($\lambda = 550$ nm). The reactions were performed in the absence (filled black circle) and presence (filled red square) of the PtOEP:DPA@PS nanoparticles, which are involved in light upconversion from green to blue light. Reaction conditions: c(Ricinoleic acid) = 5 mM, c(Cat) = 7.2 g_{CDW} L^{-1}, c(DPA) = 5 μM (**a**) or 15 μM (**b**).

oxidases and catalases) to intracellular enzymes, were used as biocatalysts. After the recombinant *E. coli* cells expressing *Cv*FAP were added into the reaction medium containing 5 or 15 μM DPA in the form of PtOEP:DPA@PS nanoparticles and 5 mM reaction substrate (**1**), green light ($\lambda = 550$ nm) was irradiated by the Xe lamp (Figure S13).

When 5 μM DPA was used for the light upconversion, (*Z*)-heptadec-9-en-7-ol (**2**) was produced to a rate of 2.5 μM/min, while the fatty alcohol (**2**) was produced to 1.4 μM/min without PS nanoparticles (Fig. 4a). This result indicated that (*Z*)-heptadec-9-en-7-ol (**2**) was produced to 1.1 μM/min via the light upconversion. Since the product concentrations reached 0.98 and 0.55 mM at t = 420 min in the presence and absence of the nanoparticles, the TONs of DPA and *Cv*FAP at t = 420 min were estimated to 86 and 72, respectively, which are significantly greater than those of isolated enzyme reaction systems (Table 1). These results suggested that the FADs in the core of *Cv*FAP enzymes, which were located in cytoplasm of the recombinant *E. coli* cells, had been quite efficiently excited by the PtOEP-DPA upconversion systems inside the poly(styrene) nanoparticles (Figure S13).

The increase of DPA concentration in PtOEP:DPA@PS nanoparticles to 15 μM led to formation of (*Z*)-heptadec-9-en-7-ol (**2**) to a rate of 3.2 μM/min (Fig. 4b). On the other hand, the fatty alcohol (**2**) was produced to 1.4 μM/min in the buffer without the PS nanoparticles, as in the experiment shown in Fig. 4b. In addition, the biotransformations in the buffer containing polystyrene nanoparticles only or DPA@PS nanoparticles only showed slightly lower product formation as compared to the biotransformation in the buffer without anything (Figure S15). Thereby, it was assumed that the target product was produced in the reaction medium to at least 1.8 μM/min via the light upconversion. The reaction rate was approximately 60% greater than that of the reaction system including 5 μM DPA as annihilator. Increased DPA concentrations in PtOEP:DPA@PS nanoparticles did not alter the TTA-UC behaviors (Figure S16). Thereby, it was assumed that the DPA concentrations have an influence on the photobiocatalytic reaction rates but did not linearly correlate.

The biotransformation of ricinoleic acid (**1**) into (*Z*)-heptadec-9-en-7-ol (**2**) was also carried out by the recombinant *E. coli* cells expressing *Cv*FAP under blue light ($\lambda = 450$ nm). The reaction rate was significantly greater than under green light ($\lambda = 550$ nm) (Figure S17), indicating that the PtOEP:DPA@PS nanoparticles need to be further improved. Thereby, the future study will focus on improvements of the TTA-UC system for enzymatic reactions in aqueous reaction systems.

Not only light-induced natural enzyme reactions but also light-dependent promiscuous enzymatic conversions have been extensively investigated for the environmentally benign synthesis of chemicals[1–5,8–10,15,18–20] and fuels[21–23]. However, as flavin catalysts utilize only a part of the wavelength spectrum of visible light (e.g., $\lambda = 450$ nm), a significant part of the energy provided by visible light remains unused. Another issue of photobiocatalysis comprises the rather poor light penetration in traditional glass-batch reactors and external illumination[50,51]. Particularly blue light ($\lambda = 450$ nm) typically penetrates no more than a few millimeters to centimeters (especially in optically dense reaction mixtures). The problem should become more serious in scale-up of the photobiocatalysis. This study demonstrated that the PtOEP:DPA@PS-based TTU-AC system can be used to partially solve the poor penetration of blue light in photobiocatalytic reactors, by enabling the enzymes to use green light ($\lambda = 550$ nm) as a light source, which is capable of penetrating deeper into the core of bioreactors without damaging the enzyme biocatalysts.

Conclusions

This study demonstrated the effectiveness of the upconversion strategy toward steering photobiocatalysis. Upconverted fluorescence emission from TTA-UC poly(styrene) nanoparticles doped with the PtOEP photosensitiser and the DPA annihilator could photoactivated FAD and FAD-bound enzymes in aqueous solutions. Combination of TTA-UC nanoparticles and bacterial cells expressing *Cv*FAP in aqueous reaction systems allowed to catalyse

decarboxylation of fatty acids into secondary fatty alcohols under green light. The results will provide useful guidance to synthetic application of photobiocatalysis.

Data availability

The datasets used and/or analysed during the current study available from the corresponding author on reasonable request.

Received: 18 February 2022; Accepted: 24 May 2022
Published online: 07 June 2022

References

1. Schmermund, L. *et al.* Photo-biocatalysis: Biotransformations in the presence of light. *ACS Catal.* **9**(5), 4115–4144 (2019).
2. Seel, C. J. & Gulder, T. Biocatalysis fueled by light: On the versatile combination of photocatalysis and enzymes. *ChemBioChem* **20**(15), 1871–1897 (2019).
3. Sandoval, B. A. & Hyster, T. K. Emerging strategies for expanding the toolbox of enzymes in biocatalysis. *Curr. Opin. Chem. Biol.* **55**, 45–51 (2020).
4. Lee, S. H., Choi, D. S., Kuk, S. K. & Park, C. B. Photobiocatalysis: Activating redox enzymes by direct or indirect transfer of photoinduced electrons. *Angew. Chem. Int. Ed.* **57**(27), 7958–7985 (2018).
5. Yi, D. *et al.* Recent trends in biocatalysis. *Chem. Soc. Rev.* **50**(14), 8003–8049 (2021).
6. Yu, Y. *et al.* Development of Synechocystis sp. PCC 6803 as a phototrophic cell factory. *Mar. Drugs* **11**(8), 2894–916 (2013).
7. Jareonsin, S. & Pumas, C. Advantages of heterotrophic microalgae as a host for phytochemicals production. *Front. Bioeng. Biotechnol.* **9**, 628597 (2021).
8. Nakano, Y. *et al.* Photoenzymatic hydrogenation of heteroaromatic olefins using 'Ene'-reductases with photoredox catalysts. *Angew. Chem. Int. Ed.* **59**(26), 10484–10488 (2020).
9. Biegasiewicz, K. F. *et al.* Photoexcitation of flavoenzymes enables a stereoselective radical cyclization. *Science* **364**(6446), 1166–1169 (2019).
10. Page, C. G. *et al.* Quaternary charge-transfer complex enables photoenzymatic intermolecular hydroalkylation of olefins. *J. Am. Chem. Soc.* **143**(1), 97–102 (2021).
11. Cheng, F. *et al.* Light-driven deracemization of phosphinothricin by engineered fatty acid photodecarboxylase on a gram scale. *Green Chem.* **22**(20), 6815–6818 (2020).
12. Huang, X. *et al.* Photoenzymatic enantioselective intermolecular radical hydroalkylation. *Nature* **584**(7819), 69–74 (2020).
13. Le, T.-K. *et al.* Solar-driven biocatalytic C-hydroxylation through direct transfer of photoinduced electrons. *Green Chem.* **21**(3), 515–525 (2019).
14. Blossom, B. M. *et al.* Photobiocatalysis by a lytic polysaccharide monooxygenase using intermittent illumination. *ACS Sustain. Chem. Eng.* **8**(25), 9301–9310 (2020).
15. Zhang, W. *et al.* Photobiocatalytic synthesis of chiral secondary fatty alcohols from renewable unsaturated fatty acids. *Nat. Commun.* **11**(1), 2258 (2020).
16. Hofler, G. T. *et al.* A Photoenzymatic NADH regeneration system. *ChemBioChem* **19**(22), 2344–2347 (2018).
17. Rauch, M. C. R. *et al.* Photochemical regeneration of flavoenzymes—An Old Yellow Enzyme case-study. *Biochim. Biophys. Acta Proteins Proteom.* **1868**(1), 140303 (2020).
18. Huijbers, M. M. E., Zhang, W., Tonin, F. & Hollmann, F. Light-driven enzymatic decarboxylation of fatty acids. *Angew. Chem. Int. Ed.* **57**(41), 13648–13651 (2018).
19. Cha, H. J. *et al.* Whole-cell photoenzymatic cascades to synthesize long-chain aliphatic amines and esters from renewable fatty acids. *Angew. Chem. Int. Ed.* **59**(18), 7024–7028 (2020).
20. Ma, Y. *et al.* Production of fatty alcohols from non-edible oils by enzymatic cascade reactions. *Sustain. Energy Fuels* **4**(8), 4232–4237 (2020).
21. Bruder, S., Moldenhauer, E. J., Lemke, R. D., Ledesma-Amaro, R. & Kabisch, J. Drop-in biofuel production using fatty acid photodecarboxylase from *Chlorella variabilis* in the oleaginous yeast *Yarrowia lipolytica*. *Biotechnol. Biofuels* **12**, 202 (2019).
22. Amer, M. *et al.* Low carbon strategies for sustainable bio-alkane gas production and renewable energy. *Energy Environ. Sci.* **13**(6), 1818–1831 (2020).
23. Ma, Y. *et al.* Photoenzymatic production of next generation biofuels from natural triglycerides combining a hydrolase and a photodecarboxylase. *ChemPhotoChem* **4**(1), 39–44 (2019).
24. Baluschev, S. *et al.* Blue-green up-conversion: Noncoherent excitation by NIR light. *Angew. Chem. Int. Ed.* **46**(40), 7693–7696 (2007).
25. Singh-Rachford, T. N. *et al.* Supermolecular-chromophore-sensitized near-infrared-to-visible photon upconversion. *J. Am. Chem. Soc.* **132**(40), 14203–14211 (2010).
26. Mongin, C., Garakyaraghi, S., Razgoniaeva, N., Zamkov, M. & Castellano, F. N. Direct observation of triplet energy transfer from semiconductor nanocrystals. *Science* **351**(6271), 369–372 (2016).
27. Liu, Q. *et al.* A general strategy for biocompatible, high-effective upconversion nanocapsules based on triplet–triplet annihilation. *J. Am. Chem. Soc.* **135**(13), 5029–5037 (2013).
28. Mahato, P., Monguzzi, A., Yanai, N., Yamada, T. & Kimizuka, N. Fast and long-range triplet exciton diffusion in metal-organic frameworks for photon upconversion at ultralow excitation power. *Nat. Mater.* **14**(9), 924–930 (2015).
29. Askes, S. H., Brodie, P., Bruylants, G. & Bonnet, S. Temperature dependence of triplet–triplet annihilation upconversion in phospholipid membranes. *J. Phys. Chem. B* **121**(4), 780–786 (2017).
30. Kim, J. H. & Kim, J. H. Encapsulated triplet–triplet annihilation-based upconversion in the aqueous phase for sub-band-gap semiconductor photocatalysis. *J. Am. Chem. Soc.* **134**(42), 17478–17481 (2012).
31. Amemori, S., Sasaki, Y., Yanai, N. & Kimizuka, N. Near-infrared-to-visible photon upconversion sensitized by a metal complex with spin-forbidden yet strong S0–T1 absorption. *J. Am. Chem. Soc.* **138**(28), 8702–8705 (2016).
32. Sasaki, Y. *et al.* Near-infrared optogenetic genome engineering based on photon-upconversion hydrogels. *Angew. Chem. Int. Ed.* **58**(49), 17827–17833 (2019).
33. Khnayzer, R. S. *et al.* Upconversion-powered photoelectrochemistry. *Chem. Commun. (Camb)* **48**(2), 209–211 (2012).
34. Kwon, O. S., Kim, J. H., Cho, J. K. & Kim, J. H. Triplet–triplet annihilation upconversion in CdS-decorated SiO_2 nanocapsules for sub-bandgap photocatalysis. *ACS Appl. Mater. Interfaces* **7**(1), 318–325 (2015).
35. Ravetz, B. D. *et al.* Photoredox catalysis using infrared light via triplet fusion upconversion. *Nature* **565**(7739), 343–346 (2019).
36. Monguzzi, A. *et al.* Efficient broadband triplet–triplet annihilation-assisted photon upconversion at subsolar irradiance in fully organic systems. *Adv. Funct. Mater.* **25**(35), 5617–5624 (2015).

37. Askes, S. H., Kloz, M., Bruylants, G., Kennis, J. T. & Bonnet, S. Triplet–triplet annihilation upconversion followed by FRET for the red light activation of a photodissociative ruthenium complex in liposomes. *Phys. Chem. Chem. Phys.* **17**(41), 27380–27390 (2015).
38. Liu, Q., Yang, T., Feng, W. & Li, F. Blue-emissive upconversion nanoparticles for low-power-excited bioimaging in vivo. *J. Am. Chem. Soc.* **134**(11), 5390–5397 (2012).
39. Kwon, O. S. *et al.* Dual-color emissive upconversion nanocapsules for differential cancer bioimaging in vivo. *ACS Nano* **10**(1), 1512–1521 (2016).
40. Liu, Q. *et al.* Highly photostable near-IR-excitation upconversion nanocapsules based on triplet–triplet annihilation for in vivo bioimaging application. *ACS Appl. Mater. Interfaces* **10**(12), 9883–9888 (2018).
41. Huang, L., Le, T., Huang, K. & Han, G. Enzymatic enhancing of triplet–triplet annihilation upconversion by breaking oxygen quenching for background-free biological sensing. *Nat. Commun.* **12**(1), 1898 (2021).
42. Wohnhaas, C. *et al.* Annihilation upconversion in cells by embedding the dye system in polymeric nanocapsules. *Macromol. Biosci.* **11**(6), 772–778 (2011).
43. Sorigue, D. *et al.* An algal photoenzyme converts fatty acids to hydrocarbons. *Science* **357**(6354), 903–907 (2017).
44. Xu, J. *et al.* Light-driven kinetic resolution of alpha-functionalized carboxylic acids enabled by an engineered fatty acid photodecarboxylase. *Angew. Chem. Int. Ed.* **58**(25), 8474–8478 (2019).
45. Zhang, C., Pansare, V. J., Prud'homme, R. K. & Priestley, R. D. Flash nanoprecipitation of polystyrenenanoparticles. *Soft Matter* **8**(1), 86–93 (2012).
46. Monguzzi, A., Frigoli, M., Larpent, C., Tubino, R. & Meinardi, F. Low-power-photon up-conversion in dual-dye-loaded polymer nanoparticles. *Adv. Funct. Mater.* **22**(1), 139–143 (2012).
47. Monguzzi, A. *et al.* Unraveling triplet excitons photophysics in hyper-cross-linked polymeric nanoparticles: Toward the next generation of solid-state upconverting materials. *J. Phys. Chem. Lett.* **7**(14), 2779–2785 (2016).
48. Karstens, T. & Kobs, K. J. Rhodamine B and rhodamine 101 as reference substances for fluorescence quantum yield measurements. *J. Phys. Chem.* **84**, 1871–1872 (1980).
49. Heyes, D. J. *et al.* Photochemical mechanism of light-driven fatty acid photodecarboxylase. *ACS Catal.* **10**(12), 6691–6696 (2020).
50. Hobisch, M. *et al.* Internal illumination to overcome the cell density limitation in the scale-up of whole-cell photobiocatalysis. *Chemsuschem* **14**, 3219–3225 (2021).
51. Duong, H. T. *et al.* Intensification of photobiocatalytic decarboxylation of fatty acids for the production of biodiesel. *ChemSusChem* **14**(4), 1053–1056 (2021).

Acknowledgements

This work was supported by the National Research Foundation of Korea (NRF) grants funded by the Korea government (MEST) (Nos. 2020R1A2B5B03002376 and 2019R1A2C2003969).

Author contributions

J.P. and Y.Y. wrote the main manuscript text and S.H. and D.S. leaded formal analysis and prepared Figs. 1, 2, 3 and 4. E.S. supported formal analysis and F.H. supported the main manuscript text. All authors reviewed the manuscript.

Competing interests

The authors declare no competing interests.

Additional information

Supplementary Information The online version contains supplementary material available at https://doi.org/10.1038/s41598-022-13406-8.

Correspondence and requests for materials should be addressed to Y.Y. or J.-B.P.

Reprints and permissions information is available at www.nature.com/reprints.

Publisher's note Springer Nature remains neutral with regard to jurisdictional claims in published maps and institutional affiliations.